JCTC Journal of Chemical Theory and Computation

New General Tools for Constrained Geometry Optimizations

Luca De Vico

Department of Theoretical Chemistry, Lund University, Chemical Centre, P.O. Box 124, S-221 00 Lund, Sweden

Massimo Olivucci*

Dipartimento di Chimica, Università di Siena, via A. De Gasperi 2, I-53100 Siena, Italy, and Centro per lo Studio dei Sistemi Complessi, Via Tommaso Pendola 37, I-53100 Siena, Italy

Roland Lindh*

Department of Chemical Physics, Lund University, Chemical Centre, P.O. Box 124, S-221 00 Lund, Sweden

Received April 8, 2005

Abstract: A modification of the constrained geometry optimization method by Anglada and Bofill (Anglada, J. M.; Bofill, J. M. *J. Comput. Chem.* **1997**, *18*, 992−1003) is designed and implemented. The changes include the choice of projection, quasi-line-search, and the use of a Rational Function optimization approach rather than a reduced-restricted-quasi-Newton−Raphson method in the optimization step. Furthermore, we show how geometrical constrains can be implemented in an approach based on nonredundant curvilinear coordinates avoiding the inclusion of the constraints in the set of redundant coordinates used to define the internal coordinates. The behavior of the new implementation is demonstrated in geometry optimizations featuring single or multiple geometrical constraints (bond lengths, angles, etc.), optimizations on hyperspherical cross sections (as in the computation of steepest descent paths), and location of energy minima on the intersection subspace of two potential energy surfaces (i.e. minimum energy crossing points). In addition, a novel scheme to determine the crossing point geometrically nearest to a given molecular structure is proposed.

1. Introduction

Whereas the standard (i.e. unconstrained) optimization of equilibrium structures on the potential energy surface (PES) is considered a relatively easy task, the optimization of transition structures and constrained geometry optimizations represent a more complex problem. For a survey of currently established methods for optimizing minima and transition state structures see refs 1 and 2 and references therein. For certain applications as, for example, the location of a minimum on a PES hyperspherical cross section (e.g. used for mapping steepest descent paths)[3] or of a stationary point located along the intersection subspace of two or more PESs[4] the implementation of novel efficient constrained optimization methods is highly desirable.

In addition to projection methods[5] and penalty functions[6] based methods, constrained geometry optimizations are mostly based on variations of the Lagrange multiplier method.[4,7,8] Here the space is extended from $3n$-6(5) to $3n$-6(5)+m, where n is the number of atoms and m is the number

* Corresponding authors e-mail: olivucci@unisi.it (M.O.) and Roland.Lindh@chemphys.lu.se (R.L.).

10.1021/ct0500949 CCC: $30.25
Published on Web 07/09/2005

of constraints. For each constraint the Hessian of the Lagrangian carries a negative eigenvalue. However, when locating a minimum energy crossing point (MECP),[4,7] the Lagrange multiplier method can sometime, in our and others[5] experience, show poor convergence, and the reason for this is associated with the Hessian. In fact (1) the separation of the space into the constraint subspace and the disjoint subspace, in which the optimization is carried out, is, in standard quasi-Newton max−min optimizations,[9] defined implicitly by the eigenvectors of the Hessian of the Lagrangian, and (2) the so-called Broyden−Fletcher−Goldfarb−Shanno (BFGS)[10] Hessian update method cannot be exploited because the Lagrangian Hessian is not positive definite.

The first matter is under control in standard optimization with geometrical constraint(s), since here the second-order derivative of the constraint(s) with respect to the internal coordinates can be computed without much effort. However, in the location of a MECP, the computation of second-order derivatives would be an impractical and expensive procedure. Hence, constrained optimizations to locate MECPs are performed with approximate Hessian in combination with Hessian update methods.

An alternative to the Lagrange multiplier method was proposed by Bearpark et al.[5] In this approach, the so-called "direct" approach, the subspace of the constraint(s), is identified to first order and treated separately from the rest of the optimization. However, the minimization is still performed in the full space in combination with projection operators. The major advantage of the "direct" approach is that the definition of the subspace of the constraint(s) is not implicitly defined by the Hessian of the Lagrangian but rather from the gradient of the constraint(s) with respect to the nuclear displacements.

Recently Anglada and Bofill[11] described the connection between the "direct" and the Lagrange multiplier approach. They demonstrated that the Lagrange multiplier method can, by a simple linear transformation, be recast into *one subspace of the constraint(s) (of dimension m) and one geometrical coordinate subspace (of* dimension 3*n*-6(5)-*m*) in which a minimization is performed. *The latter is guaranteed to have a positive definite* Hessian. Hence, it combines the advantage of space subdivision, as suggested by the so-called direct approach, with a conventional minimization in combination with a BFGS Hessian update procedure. The method was implemented in the semiempirical program package AMPAC[12] and tested in combination with the AM1 Hamiltonian,[13] using a reduced-restricted-quasi-Newton−Raphson method and explicit line-search techniques.

The combination of general geometrical constraints with optimizations in Cartesian internal coordinates is trivial.[14] While a scheme for constrained optimizations in conjunction with curvilinear internal coordinates has been suggested by Baker et al.,[15] this requires that the geometrical constraint(s) are included in the coordinate space. It would be of advantage if the constraint(s) could be excluded from the coordinate space since they do not usually qualify as a natural internal coordinate.

In this paper we will explore the method of Anglada and Bofill, in combination with the Rational Function approach[16] and no line-search techniques. The method will be assessed at the (state average) CASSCF level of theory (even if any kind of level of theory could have been used, given that it was suitable for the studied system) and in combination with force-constant weighted redundant internal coordinates[17] and Hessian model function[18] implemented in the MOLCAS 6.0 quantum chemistry program package.[19,20] Further modifications of the approach will be suggested, and it will be demonstrated how constraints can be treated in combination with curvilinear internal coordinates and without their inclusion in the subspace of the redundant internal coordinates. In particular, we will present *an original procedure to optimize the crossing point geometrically nearest to a given* structure, that in the future will be made automatic.

2. Method

The methods section is subdivided into four parts. In the first part we will review and modify the projected constrained optimization (PCO) method of Anglada and Bofill. This is followed by an explicit description and motivation of our implementation in combination with a Rational Function optimization (RFO) and no line-search. Afterward, in the third subsection we describe the tools needed for combining arbitrary geometrical constraints with curvilinear internal coordinates. Finally, the last subsection will report some technical computational details.

2.1. The PCO Approach by Anglada and Bofill. The constrained geometry optimization using the Lagrange multiplier method is formulated as a minimization of the expression

$$L(\mathbf{q},\lambda) = E(\mathbf{q}) - \lambda^T \mathbf{r}(\mathbf{q}) \tag{1}$$

where E is the energy to be minimized with respect to the constraints $\mathbf{r}(\mathbf{q})$, and λ is the vector with the so-called Lagrange multipliers. A Taylor expansion to second order of $L(\mathbf{q}, \lambda)$ around $\mathbf{q}_0$ and λ_0 gives

$$L(\mathbf{q}_0 + \Delta\mathbf{q}, \lambda_0 + \Delta\lambda) = E(\mathbf{q}_0) + \Delta\mathbf{q}^T \frac{\partial E(\mathbf{q}_0)}{\partial \mathbf{q}} + (1/2)\Delta\mathbf{q}^T \mathbf{W} \Delta\mathbf{q} - \lambda^T \left(\mathbf{r}(\mathbf{q}_0) + \frac{\partial \mathbf{r}(\mathbf{q}_0)}{\partial \mathbf{q}} \Delta\mathbf{q} \right) \tag{2}$$

where $\mathbf{W}$ is defined as

$$\mathbf{W}(\mathbf{q}_0,\lambda_0) = \frac{\partial^2 E(\mathbf{q}_0)}{\partial \mathbf{q}^2} - \sum_{i=1,m} (\lambda_0)_i \frac{\partial^2 (\mathbf{r}(\mathbf{q}_0))_i}{\partial \mathbf{q}^2} \tag{3}$$

This sets up the equation for the generalized elimination method.[1,21] We note that the last term of the right-hand side of eq 2 controls to first order the constraint. In the subspace which fulfills the constraint any displacement $\Delta\mathbf{q}$ must be such that

$$\mathbf{r}(\mathbf{q}_0) + \frac{\partial \mathbf{r}(\mathbf{q}_0)}{\partial \mathbf{q}} \Delta\mathbf{q} = \mathbf{0} \tag{4}$$

This defines a linear transformation which will to first order subdivide the original 3*n*-6(5) space into a m-dimensional space in which the constraints are fulfilled and

a 3*n*-6(5)-*m* subspace in which a normal optimization is made. The unitary transformation matrix **T** contains two parts and transforms as

$$\Delta\mathbf{q}_0 = [\mathbf{T}_c\mathbf{T}_m]\begin{pmatrix}\Delta\mathbf{y}\\ \Delta\mathbf{x}\end{pmatrix} = \mathbf{T}_c\Delta\mathbf{y} + \mathbf{T}_m\Delta\mathbf{x} \tag{5}$$

where **y** and **x** are the new parameters. **y** is of *m* dimensions and **x** is of 3*n*-6(5)-*m* dimension. In particular we note that at $\mathbf{q}_0$

$$\frac{\partial\mathbf{r}(\mathbf{q}_0)}{\partial\mathbf{q}}\mathbf{T}_c \neq \mathbf{0} \tag{6}$$

and

$$\frac{\partial\mathbf{r}(\mathbf{q}_0)}{\partial\mathbf{q}}\mathbf{T}_m = \mathbf{0} \tag{7}$$

These two equations are sufficient for the definition of **T** via a Gram-Schmidt procedure.[22]

We now proceed by introducing the transformation matrix into the Lagrangian expression (eq 2). The equation now splits into two parts (one of *m* and a second of 3*n*-6(5)*m* dimensions), one of which depends only on **y**

$$\Delta\mathbf{y} = -\left(\frac{\partial\mathbf{r}(\mathbf{q}_0)}{\partial\mathbf{q}}\mathbf{T}_c\right)^{-1}\mathbf{r}(\mathbf{q}_0) \tag{8}$$

and a second part that depends on both **x** and **y**

$$Q(\mathbf{q}_0+\Delta\mathbf{q}) = E(\mathbf{q}_0) + \Delta\mathbf{y}^T\mathbf{T}_c{}^T\frac{\partial E(\mathbf{q}_0)}{\partial\mathbf{q}} + (1/2)\Delta\mathbf{y}^T\mathbf{T}_c{}^T\mathbf{W}\mathbf{T}_c\Delta\mathbf{y} + \Delta\mathbf{x}^T\mathbf{T}_m{}^T\left(\frac{\partial E(\mathbf{q}_0)}{\partial\mathbf{q}} + \mathbf{W}\mathbf{T}_c\Delta\mathbf{y}\right) + (1/2)\Delta\mathbf{x}^T\mathbf{T}_m{}^T\mathbf{W}\mathbf{T}_m\Delta\mathbf{x} \tag{9}$$

The latter is the so-called projected energy expression, with $\mathbf{T}_m{}^T\mathbf{W}\mathbf{T}_m$ being the reduced Hessian and $\mathbf{T}_m{}^T([\partial E(\mathbf{q}_0)]/[\partial\mathbf{q}] + \mathbf{W}\mathbf{T}_c\Delta\mathbf{y})$ is the reduced gradient. Solving eq 8 and substituting the result into eq 9 we minimize *Q* with respect to $\Delta\mathbf{x}$. The minimization of eq 9 can be done with any standard optimization technique. At convergence we have found the solution to the Lagrangian in eq 1.

Using the quasi-Newton condition applied to eq 1 we find that the effective gradient to be used in an Hessian update procedure applied only to the molecular part of the Lagrangian Hessian is

$$\mathbf{h}(\mathbf{q},\lambda) = \frac{\partial E(\mathbf{q})}{\partial\mathbf{q}} - \frac{\partial\mathbf{r}(\mathbf{q})}{\partial\mathbf{q}}\lambda \tag{10}$$

The update procedure is commenced by evaluating a series of $\mathbf{h}(\mathbf{q},\lambda)$ for different values of **q** and a fixed value of λ. A suitable value of λ is the first order estimate of λ at convergence as given by

$$\mathbf{h}(\mathbf{q}_0,\lambda_0) = \mathbf{0} \tag{11}$$

To conclude the presentation of the PCO approach of Anglada and Bofill let us here summarize the major advantages of the presented method, compared to an optimization/maximization procedure applied to eq 1: (1) the PCO approch has an explicit separation of the two subspaces, while an optimization/maximization indirectly separates the two subspaces by identifying the positive and negative eigenvectors of the Hessian of the Lagrangian, (2) the presence of negative eigenvalues in the Hessian of the Lagrangian restricts the selection of Hessian update (variable metric) methods, while the PCO approach allows the use of the BFGS update method to be applied to the reduced Hessian, and (3) the technique by Bofill and Anglada does not explicitly require λ to be determined.

In particular the first point is of importance since it allows us to perform constrained optimization in cases where we cannot or would not like to compute explicit second-order derivatives of the constraints with respect to nuclear displacement. One such important case is in the search of a minimum energy cross point (MECP) on the search of a (conical) intersection.

2.2. An RFO Implementation without Line-Search. In this section we will sketch on an implementation of the PCO approach in combination with Rational Function optimization and a back-feed mechanism rather than a line-search.

For a given $\mathbf{q}_1$ and a maximum step length of β, set $k = 1$, $y_\beta = 1$, $g_\beta = 1$, $x_\beta = 1$, $dy = \beta$, $g = \beta$, and $dx = \beta$.

(1) Compute $E(\mathbf{q}_k)$, $\frac{\partial E(\mathbf{q}_k)}{\partial\mathbf{q}}$, an empirical estimate of $\frac{\partial^2 E(\mathbf{q}_k)}{\partial\mathbf{q}^2}$, $\mathbf{r}(\mathbf{q}_k)$, $\frac{\partial\mathbf{r}(\mathbf{q}_k)}{\partial\mathbf{q}}$, and $\frac{\partial^2\mathbf{r}(\mathbf{q}_k)}{\partial\mathbf{q}^2}$

(2) For $i = 1,k$

Evaluate $\mathbf{T}(\mathbf{q}_i)$, $\Delta\mathbf{y}(\mathbf{q}_i)$, $\lambda(\mathbf{q}_i)$, $\mathbf{x}(\mathbf{q}_i)$, $\Delta\mathbf{x}(\mathbf{q}_i)$ and the reduced gradient, $\mathbf{g}_r(\mathbf{q}_i)$, as defined in previous equations.

If $dy < 0.75|\Delta\mathbf{y}|$ or $|\Delta\mathbf{y}| < 1.0\cdot10^{-2}$
set $y_\beta = \min(2, y_\beta \times \sqrt{2})$
Else if $(dy > 1.25|\Delta\mathbf{y}|)$ and $(dy \geq 1.0\cdot10^{-5})$
set $y_\beta = \max(1/10, y_\beta/\sqrt{2})$
Set $dy = |\Delta\mathbf{y}|$

and

If $i \neq k$
If $dx < |\Delta\mathbf{x}|$ and $|\Delta\mathbf{x}| < \beta$
set $x_\beta = \min(1, x_\beta \times \sqrt{2})$
Else if $dx > 1.25|\Delta\mathbf{x}|$ or $dx \geq \beta$
set $x_\beta = \max(1/5, x_\beta/\sqrt{2})$
Set $dx = |\Delta\mathbf{x}|$

and

If $g < 0.75|\mathbf{g}_r|$ and $g < \beta$
set $g_\beta = \min(1, g_\beta \times \sqrt{2})$
Else if $g > 1.25|\mathbf{g}_r|$ or $g \geq \beta$
set $g_\beta = \max(1/5, g_\beta/\sqrt{2})$
Set $g = |\mathbf{g}_r|$.

(3) For $i = 1,k$

Evaluate $\mathbf{h}(\mathbf{q}_i,\lambda_k)$ as expressed by eq 10.

(4) Compute $\mathbf{W}$ and update with the BFGS procedure.

(5) Assemble the reduced Hessian according to eq 9.

(6) Minimize Q (see eq 9) with respect to $\Delta\mathbf{x}(\mathbf{q}_k)$ with RFO in association with a step restriction of $\beta \times \max(y_\beta \times \min(x_\beta, g_\beta), (1/10))$.

(7) Evaluate $\Delta\mathbf{q}(\mathbf{q}_k)$ from $\Delta\mathbf{y}(\mathbf{q}_k)$ and $\Delta\mathbf{x}(\mathbf{q}_k)$.

(8) If not converged, set $k = k + 1$ and go to (1).

The design of this scheme has a major objective to give priority to the constraint(s) condition over the overall minimization procedure. Once the constraints are fulfilled, the algorithm will protect this condition. The implemented method was tailored in order to achieve a better convergence on some test cases. Mainly, this refinement consisted in tuning the parameters relative to the components of the step length of the two subspaces.

2.3. Derivatives of Constraints. Constrained geometry optimization requires first- and second-order derivatives of the constraint(s) with respect to the internal coordinates. This is trivial for Cartesian coordinates. For curvilinear coordinates Baker et al.[15] suggested to include the constraint(s) in the definition of the redundant internal coordinate space, followed by a linear transformation after the generation of the nonredundant coordinates, such that the coefficient(s) of the constraint(s) equals(equal) one(some) of the nonredundant coordinates. In this paper we will present the required derivatives for the case when the constraints not necessarily are explicitly expressed in the redundant space of internal coordinates.

Given

$$\frac{\partial}{\partial \mathbf{x}} = \frac{\partial}{\partial \mathbf{q}}\frac{\partial \mathbf{q}}{\partial \mathbf{x}} \tag{12}$$

The first-order derivative is expressed as

$$\frac{\partial \mathbf{r}}{\partial \mathbf{q}} = \left(\frac{\partial \mathbf{q}}{\partial \mathbf{x}}\right)^{-1}\frac{\partial \mathbf{r}}{\partial \mathbf{x}} \tag{13}$$

And the second derivative is expressed as

$$\frac{\partial^2 \mathbf{r}}{\partial \mathbf{q}^2} = \left(\frac{\partial \mathbf{q}}{\partial \mathbf{x}}\right)^{-1}\left[\frac{\partial^2 \mathbf{r}}{\partial \mathbf{x}^2} - \frac{\partial \mathbf{r}}{\partial \mathbf{q}}\frac{\partial^2 \mathbf{q}}{\partial \mathbf{x}^2}\right]\left(\frac{\partial \mathbf{q}}{\partial \mathbf{x}}\right)^{-1} \tag{14}$$

2.4. Computational Details. The method described above was used to perform constrained geometry optimizations, testing the response with constraints of various kinds. The standard thresholds of the MOLCAS SlapAf module were applied to check convergence. Namely, a RMS value of 0.12×10^{-2} au and a largest component smaller than 0.18×10^{-2} au was considered as a threshold for the Cartesian displacements; a RMS value of 0.30×10^{-3} au and a largest component smaller than 0.45×10^{-3} au was considered as a threshold for the gradient vector. All optimizations reported in the Results section were calculated at the CASSCF level of theory. Nonetheless, the method could have been applied using any level of theory, as long as it is appropriate to the studied problem. Computations in subsections 3.1 and 3.2 employed a ANO-RCC basis set[23] and a minimum active space comprising 2 electrons in 2 orbitals. The 6-31G* basis set[24] was chosen for the optimizations presented in subsections 3.3−3.6. For *N*-methylthioacetamide (NMTAA, see subsection 3.3) an active space comprising 10 electrons in 8 orbitals (see ref 25 for details on orbitals' choice) was chosen, while a minimum (6 electrons in 5 orbitals) active space comprising the π orbitals and one of the oxygen lone pairs was preferred for acrolein (subsections 3.4−3.6), respectively.

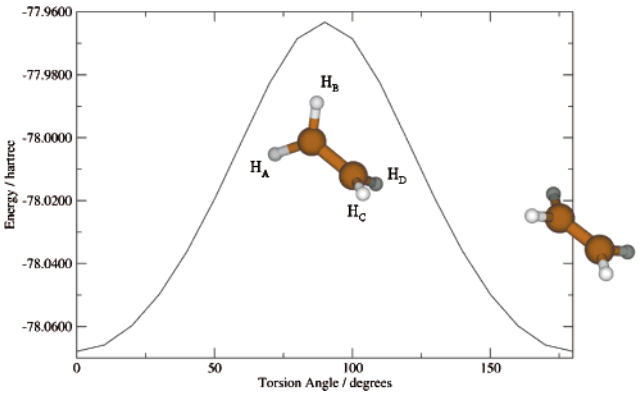

Figure 1. Ethene hindered internal rotation.

3. Results and Discussion

In this section we test the implemented method with respect to (i) geometry optimizations with single and multiple constraints, (ii) optimizations on a PES hyperspherical cross section applied to the mapping of steepest descent paths, and (iii) the optimization of MECPs.

3.1. Single and Multiple Geometrical Constraint Optimization. To evaluate the efficiency of the geometry optimization with a single geometrical constraint, we compute the energy profile for ethene double bond twisting (see Figure 1). This is done running a set of geometry optimizations where the H_ACCH_C dihedral angle is required to assume a predefined final value. Thus, the constraint is

$$r_1 = \phi_{H_ACCH_C} - \phi^0_{H_ACCH_C} \tag{15}$$

On average, we find that the optimizations converge after 6 iterations for each selected angle.

To evaluate if this efficiency is maintained in the case of an increased number of geometrical constrained, we have mapped a two-dimensional cross section of the triplet potential energy surface of the 1,2-dioxoethane biradical. This has been carried out running a grid of geometry optimizations where the O−O bond distance and the O−C−C−O dihedral angle are required to assume predefined final values (see surface in Figure 2). In this case the constraints are

$$r_1 = r_{OO} - r_{OO}{}^0 \tag{16}$$

and

$$r_2 = \phi_{OCCO} - \phi_{OCCO}{}^0 \tag{17}$$

As for the case of a single constraint we have found that each optimization typically converge after 5 iterations.

3.2. Steepest Descent Path Optimizations. Steepest descent paths can be constructed by using a variety of algorithms, see ref 2 and references therein. We chose to

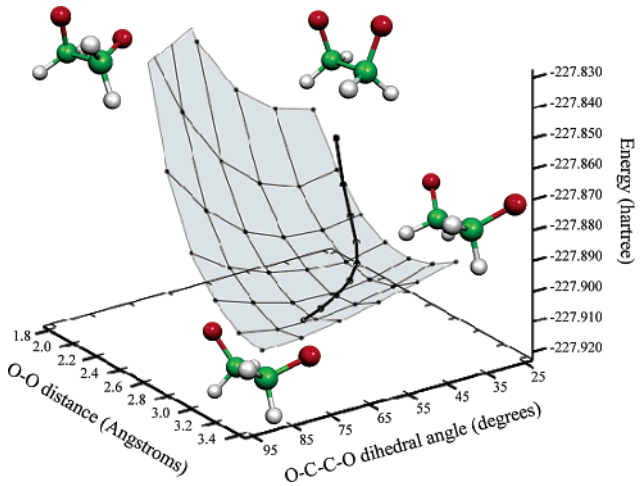

Figure 2. The potential energy surface of triplet 1,2-dioxetane as a function of the O−O bond distance (angstrom) and the O−C−C−O dihedral angle (degrees), shaded surface. Each point of the grid was obtained through the procedure described in section 3.1. The minimum energy path of 1,2-dioxoethane on the same state surface starting at the geometry of the singlet transition state is also reported in black line. The method used to calculate the path is described in section 3.2. The first part of the path (higher energy) is mainly characterized by the O−O stretching coordinate, while the second part (lower energy) is mostly described by the O−C−C−O dihedral torsional coordinate.

follow a Müller−Brown approach[26] and construct them through a series of geometry optimizations, each requiring the minimization of the potential energy on a hyperspherical cross section of the PES centered on a given reference geometry and characterized by a predefined radius. One usually starts the calculation from a high energy reference geometry, which may correspond to the Franck−Condon structure on an excited-state PES or to a transition structure (TS). Once the first lower energy optimized structure is converged, this is taken as the new hypersphere center, and the procedure is iterated until the bottom of the energy surface is reached. Notice that in the TS case a pair of steepest descent paths, connecting the TS to the reactant and product structures (i.e. following the forward and reverse orientation of the direction defined by the transition vector) provides the minimum energy path (MEP) for the reaction. If mass-weighted coordinates $\mathbf{R}(\mathbf{q})$ are used, the MEP coordinate corresponds to the so-called Intrinsic Reaction Coordinates (IRC).

$$\mathbf{R}(\mathbf{q}) = (\sqrt{m_1}\mathbf{r}_1(\mathbf{q}),\sqrt{m_2}\mathbf{r}_2(\mathbf{q}),...,\sqrt{m_n}\mathbf{r}_n(\mathbf{q})) \qquad (18)$$

Choosing this type of coordinates our methods requires that the following constrain is satisfied at the end of the optimization

$$r_1 = \frac{\sqrt{(\mathbf{R}(\mathbf{q}) - \mathbf{R}(\mathbf{q}_{\mathrm{ref}}))^2} - R}{\sqrt{M_{\mathrm{tot}}}} \qquad (19)$$

where $\mathbf{R}$ is the radius of the hypersphere and M_{tot} is the total mass of the system.

The performance of our implementation is, again, assessed on the triplet 1,2-dioxoethane biradical. As a starting geometry we take that of the syn singlet biradical structure that defines the transition state for the ring-opening of dioxethane. A hypersphere radius of 0.1 au was chosen. A small value for the radius implies not only less iterations before convergence is reached but also a larger number of points to be calculated to describe the MEP. We found that 0.1 au represents a balanced value to calculate the entire MEP. As we show in Figure 2 the steepest descent path in mass-weighted coordinates is easily constructed even in the presence of a turn in the path coordinate. Each individual optimization typically takes 9 iterations to converge.

3.3. Optimization of Minimum Energy Crossing Points: Nongeometrical Constraints. A MECP is computed by optimizing the structure corresponding to a local excited state (e.g. E_1) energy minimum requiring that a degeneracy constraint with a lower potential energy surface (e.g. E_0) is satisfied at the end of the optimization. Thus the constraint is the energy difference between the two electronic states:

$$r_1 = E_1 - E_0 \qquad (20)$$

Notice that in this case the required constraint is not geometrical. To test the methodology we compute the intersection between the ^{3}A and ^{1}A state of *N*-methylthioacetamide (NMTAA).

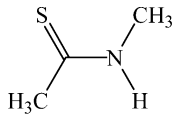

N-methylthioacetamide

NMTAA was chosen as a test molecule for calculating MECP because, as reported in a recent paper,[25] we failed to obtain fully optimized singlet/triplet crossings of this molecule by using other methods. The changes of the excited-state energy (E_1) and of the energy difference (r_1) as a function of the number of iteration (Figure 3) display a fast convergence (in about five iterations, both energy difference and excited state energy are nearly converged).

3.4. Multiple Heterogeneous Constraints: MECP Search on an Hyperspherical Cross Section. *The ultimate target of the test presented in this section is to compute the crossing point geometrically closest to a given molecular structure.* To achieve this target two qualitatively different (heterogeneous) types of constraints are imposed during the optimization. The first constraint determines the value of the E_1-E_0 energy difference as seen in section 3.3 above. The second constraint is of the type described in section 3.2 and corresponds to the distance between the target geometry and a given reference molecular structure. Recently, we presented a method[27] for searching PES crossing points over a hyperspherical cross section, not directly based on Lagrangian multipliers. Even if it has been used in various cases,[28] it needed some tailoring specific for each considered molecular system. The present method, on the other hand, should be more generally applicable.

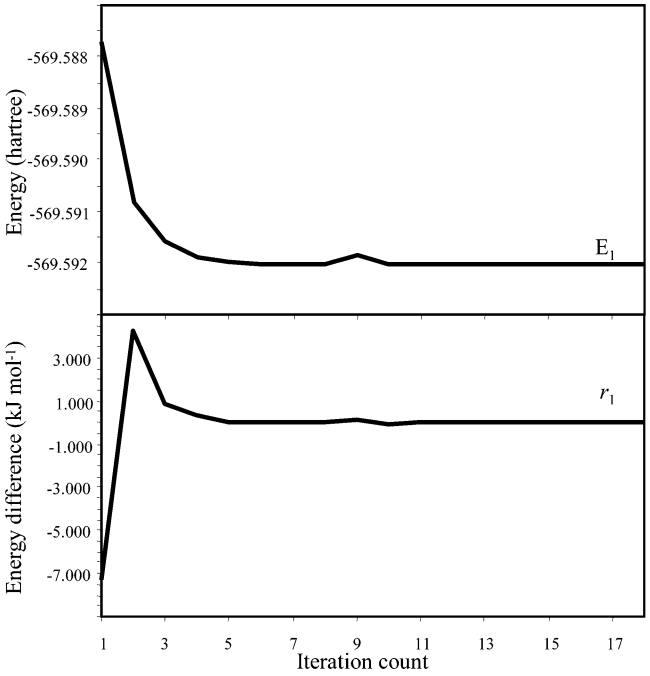

Figure 3. The excited triplet state energy of *N*-methylthioacetamide (indicated as E_1, see text) and the energy difference (indicated as *r*, see eq 20) as a function of the iteration count during the MECP optimization.

Due to its considerable experimental and theoretical interest,[29,30] the simple conjugated carbonyl compound acrolein was chosen for our test. Accordingly, the chosen reference structure is the previously reported[30] ^{3}n-π* planar minimum of the fundamental triplet state (T_1). Notice that the target structure, i.e., the acrolein crossing point geometrically closest to the selected reference, will, in general, not correspond to a MECP.

As will become clear later, the present implementation of our optimization scheme for finding the T_1/S_0 crossing point nearest (NCP) to the reference T_1 minimum, is not automatic but is based on a series of sequential *singlet/triplet energy difference minimization coupled to a geometry minimization on a hyperspherical cross section of the T_1 energy surface. Each optimization is characterized by a different value of the hypersphere radius that is regularly decreased along the series.* As seen in the previous sections, the two constraints to be applied in each optimization are

$$r_1 = E_1 - E_0 \tag{21}$$

$$r_2 = \frac{\sqrt{(\mathbf{R}(\mathbf{q}) - \mathbf{R}(\mathbf{q}_{\text{ref}}))^2} - R}{\sqrt{M_{\text{tot}}}} \tag{22}$$

At the end of the optimization the r_1 and r_2 values must be zero. More specifically, given a hyperspherical cross section of the PES defined by the radius *R* and assuming that the *N*-1-dimensional T_1/S_0 intersection subspace (where *N* is the number of freedom degrees, equal to 3*n*-6) we look for a structure belonging to the T_1/S_0 intersection and having the lowest possible T_1 energy. As displayed in Figure 4, where one optimization step is analyzed, about 5 iterations were sufficient to achieve nearly convergence.

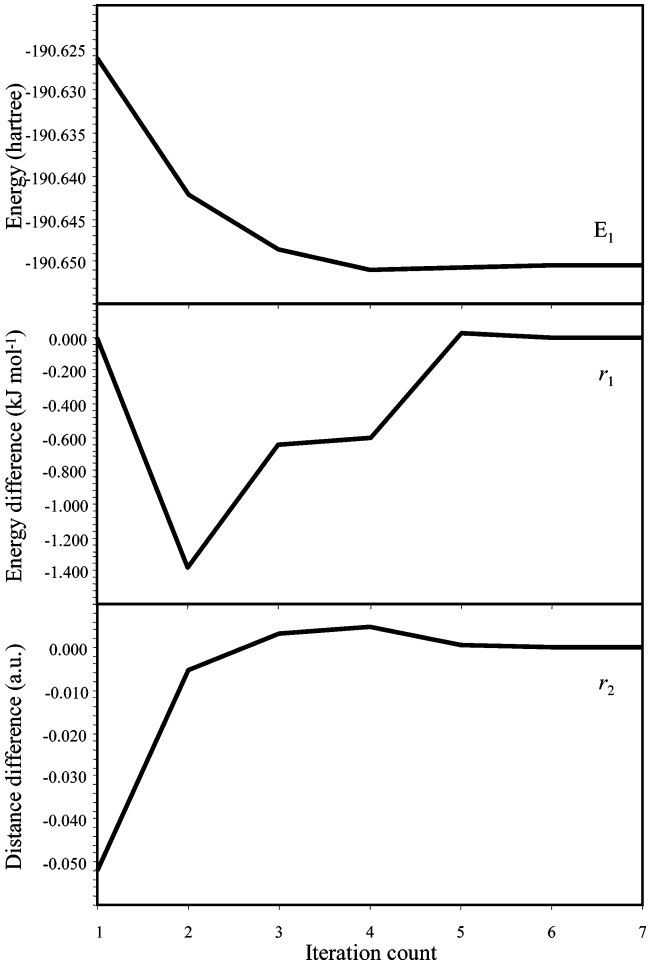

Figure 4. Energy of the ^{3}n-π* state (indicated as E_1, see text), energy difference (indicated as r_1, see eq 21), and distance difference from the constrained value (indicated as r_2, see eq 22) as a function of iteration count during the optimization of the point of the ^{3}n-π*/S_0 seam at 0.35 au from the T_1 planar minimum (see Figure 5).

As anticipated above, the minimization of *R* was performed "manually". To better follow such procedure and provide an initial guess we optimized, following the method described in section 3.3, the T_1/S_0 MECP. The optimization yielded a structure located 7 kcal mol^{-1} below the reference ^{3}n-π* T_1 minimum that shows a twist of 93.3° degrees around the C═C bond, a lengthening of C═C and C−C bonds, and shortening of the C═O bond, with respect to the reference. Moreover, such MECP connects the $^3\pi-\pi$* potential energy surface to that of the singlet ground state and is not related to the ^{3}n-π* state. The first optimization was performed taking a radius smaller than the 0.462 au distance between the reference and the MECP guess. Once an optimized geometry was obtained, its structure was used as starting geometry for the following optimization with a shorter *R*. The procedure was iterated until it was not possible to achieve convergence: at this stage the hyperspherical cross section was no more intersecting the T_1/S_0 intersection subspace. *The final NCP structure, corresponding to a ^{3}n-π*/S_0 crossing, was located 0.228 au from and 108 kcal mol^{-1} higher in energy with respect to the reference T_1 planar minimum, Its geometrical parameters are reported*

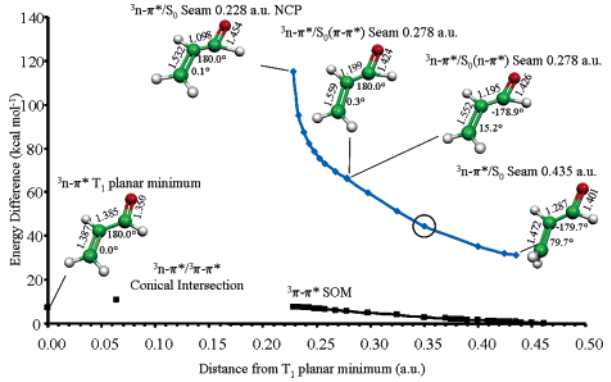

Figure 5. Acrolein, ^{3}n-π* T$_1$ planar minimum, ^{3}n-π*/S$_0$ NCP, ^{3}n-π*/$^3\pi$-π* conical intersection,[30] ^{3}n-π*/S$_0$ seam (full diamonds, blue line), $^3\pi$-π* SOM (series of minima, full squares, black line). All geometrical parameters are in angstrom and degrees. The optimization of the circled point of the ^{3}n-π*/S$_0$ seam at 0.35 au from the T$_1$ planar minimum is the one analyzed in Figure 4. The SOM points represent a path in the $^3\pi$-π* valley, even if they were not calculated as a rigorous IRC or steepest descent path. See section 3.6.

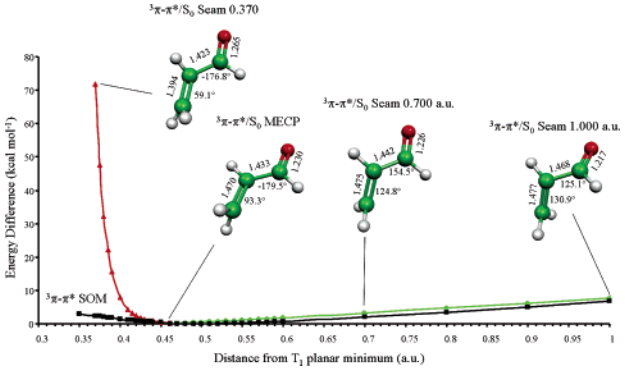

Figure 6. Acrolein, $^3\pi$-π*/S$_0$ seam (full triangles, red line plus full circles, green line), and $^3\pi$-π* SOM (full squares, black line). All geometrical parameters are in angstrom and degrees.

in Figure 5. Given the energy difference with the reference planar minimum and the unusual structure (see the C−C distance of 1.098 Å), it is very unlikely that the NCP structure could be physically reached.

The location of the NCP to a given structure may be important when investigating a photochemical process. In fact, it can give an idea of the accessibility of a certain crossing seam from a previously optimized excited-state intermediate (an energy minimum) or excited-state reaction path (a steepest descent path). *In the future, an algorithm to perform a simultaneous minimization of r_1, r_2, and of the radius (R) will be implemented, to provide a tool to locate, in an unbiased way, the geometrically NCP to a given structure.*

3.5. Mapping the Intersection Subspace: the ^{3}n-π*/S$_0$ Seam. The methodology used in section 3.4 can also be used to construct a low-lying ^{3}n-π*/S$_0$ cross section of the *N*-1-dimensional ^{3}n-π*/S$_0$ intersection space that originate at NCP. Taking the T$_1$ planar minimum as the hypersphere center we run a series of two-constraint (r_1 and r_2 as seen above) optimizations setting a hypersphere radius longer than 0.228 au and pointing in the direction of the optimized NCP. The optimized structure was then used as the guess geometry for the next optimization at an even longer radius and maintaining the planar minimum as the hypersphere center. The ^{3}n-π*/S$_0$ seam reported in Figure 5 was built in this way (blue line).

Notice that at the beginning of the seam the optimized structures are planar, showing only stretching distortions: C═C and C═O lengthening and C−C shortening, with respect to the T$_1$ planar minimum. Around 0.278 au twisting around C═C begins, along with inversion of the stretching movements. Actually, two different structures with nearly degenerate energies where found at 0.278 au distance. A change in the S$_0$ wave function, from a partial $\pi-\pi$* character to a partial n-π* character is likely to be at the basis of such a behavior. More specifically, it could happen that a ^{1}n-π*/$^1\pi-\pi$* seam crosses the located singlet/triplet seam. The ^{3}n-π*/S$_0$ seam ends (approximately) at 0.435 au as at longer distances the optimization leads, as explained below, to a $^3\pi-\pi$*/S$_0$ seam, that is lower in energy.

3.6. Mapping the Intersection Subspace: the $^3\pi$-π*/S$_0$ Seam. The existence of crossing points with $^3\pi-\pi$*/S$_0$ character (e.g. the MECP documented in section 3.4) and located lower in energy than any point of the ^{3}n-π*/S$_0$ seam documented in section 3.5 suggests that the low-energy region of T$_1$ must be dominated by a $\pi-\pi$* character. This is confirmed by relaxation of the ^{3}n-π*/S$_0$ seam point on T$_1$. In fact, a set of low-lying $^3\pi-\pi$* point (SOM) were located performing a series of standard T$_1$ geometry optimizations on hyperspherical cross sections (as discussed in section 3.2) centered on the usual T$_1$ planar minimum and starting at each ^{3}n-π*/S$_0$ seam point (i.e. using the same radius and hypersphere center of the seam). The optimized points are shown in Figure 5 (black line). Clearly, the SOM represents a sort of bottom of the T$_1$ valley closest to the computed ^{3}n-π*/S$_0$ seam. In other words, SOM is a scan of the T$_1$ potential energy surface at various distances from the T$_1$ planar minimum. Since it is a scan, it may not have the same properties of an IRC or MEP. Remarkably, it was found (via orbital occupancy analysis) that the T$_1$ SOM has a $^3\pi-\pi$* nature. The low-lying regions of the T$_1$ potential energy surface showing a $^3\pi-\pi$* and ^{3}n-π* character (as the ^{3}n-π* planar minimum in Figure 5) must be somehow connected. In Figure 5 we report the energy of a previously located ^{3}n-π*/$^3\pi-\pi$* conical intersection[30] that may provide a link between these two T$_1$ regions.

The existence of a low-lying $^3\pi-\pi$* region suggests the existence of a low-lying $^3\pi-\pi$*/S$_0$ seam. To locate such a seam we employed the same procedure used to locate the NCP point (see section 3.4) but starting with a longer radius. In fact, the computations were started at the structure of MECP (at 0.462 au from the usual hypersphere center) and performing iteratively a series of two constraints (r_1 and r_2) minimizations of the T$_1$ energy with a decreased or increased radius. The seam, reported in Figure 6 along with the T$_1$ SOM, is divided into two branches, characterized by shorter or longer *R* values. The branch on the left of the figure (red line) is characterized by twisting of the C═C bond mixed with C═C and C−C lengthening and C═O shortening. The branch on the right side (green line) is substantially an

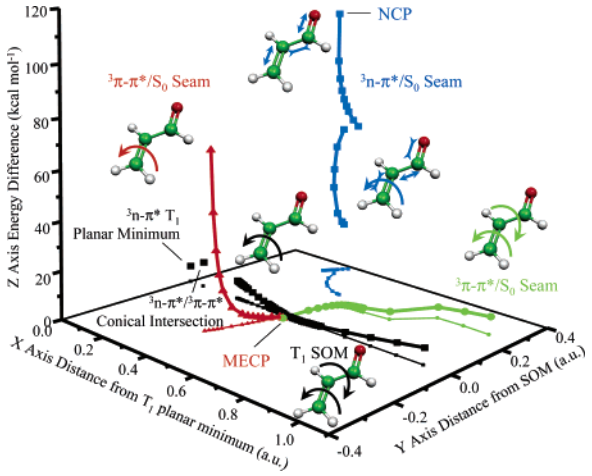

Figure 7. Acrolein, general view of the calculated seams, with relative distance from the corresponding points of the SOM. Arrows on the molecular structures represent the main movement characterizing each branch of the seams or the SOM. As stated in section 3.5, the ^{3}n-π^*/S_0 intersection seam is split in two parts, each characterized by different skeletal movements. The two degenerate structures at 0.278 au from the T_1 planar minimum do not have the same distance from SOM, originating two separate branches.

extension of the previous one both from the geometrical and electronic structure point of view. However, this branch features an additional twisting about the C−C bond, which leads to quite distorted structures. Notice the SOM curve and the right branch of the seam go along nearly in parallel and close to each other, being the energy difference between them never more than 1.5 kcal mol^{-1}. The point of the SOM at 0.490 au from the T_1 planar minimum has the lowest energy of all the computed structures. The energies of all structures reported in Figures 5−7 were calculated as difference with respect to that of this structure.

The difference in energy is not the only important parameter to be considered when comparing seams and valleys (even if SOM does not rigorously correspond to a valley). In fact, the difference in geometry provides information on the vibrational modes that most effectively could lead from the T_1 valley to the seam and, therefore, to intersystem crossing. The computed distances between the equivalent (i.e. featuring the same radius R from the reference T_1 planar minimum) points of the seams and SOM are summarized in Figure 7. The seams as well as the SOM follow the same coloring/symbol as in Figures 5 and 6 and the distance from the T_1 planar minimum is reported on the X axis. Similarly, the distances of the seam points from the corresponding SOM points are given on the Y axis. The projection on the XY plane is also reported, and it is indicated by smaller symbols. The energy difference is on the Z axis. As can be seen, being close in energy does not imply being close geometrically. It is also interesting to note that our results suggest that only the crossing points located in the vicinity of the MECP point could be vibrationally accessible at room temperature from the T_1 state. A more quantitative evaluation of such accessibility including quantum effects would require a more rigorous and expensive procedure and is out of the scope of this paper.

4. Conclusions

A modified algorithm based on the approach of Anglada and Bofill has been implemented and tested. The results indicate that such implementation can be used with success in different cases of constrained geometry optimizations. It has been shown that geometry optimizations subject to both geometrical and energy constraints are efficient. Most remarkably, we have provided evidence that geometry optimization in the presence of multiple and heterogeneous constraints (i.e. simultaneous geometrical and energy constraints) is also efficient. This last features allows for the mapping of very different and complex seams of intersection relating electronic states of different electronic nature with the ground state. In the present paper, only crossings between singlet and triplet state surfaces have been optimized. Nevertheless, the developed method is generally valid for any kind of constraint. Work on exploring the new optimization tools in connection with conical intersection optimization problems is in progress.

Acknowledgment. The authors wish to thank the Università di Siena (Progetto di Ateneo A.A. 02/04), the Swedish Research Council (VR), and the Swedish Foundation for Strategic Research (SSF).

References

(1) Gill, P. E.; Murray, W. In *Numerical Methods for Constrained Optimization*; Gill, P. E., Murray, W., Eds.; Academic Press: London, 1974.

(2) Schlegel, H. B. *J. Comput. Chem.* **2003**, *24*, 1514−1527.

(3) Fukui, K. *Acc. Chem. Res.* **1981**, *14*, 363. Gonzales, C.; Schlegel, H. B. *J. Chem. Phys.* **1991**, *95*, 5853.

(4) Koga, N.; Morokuma, K. *Chem. Phys. Lett.* **1985**, *119*, 371.

(5) Bearpark, M. J.; Robb, M. A.; Schlegel, H. B. *Chem. Phys. Lett.* **1994**, *223*, 269−274.

(6) Fletcher, R. *Practical Methods of Optimization: Constrained Optimization*; Wiley & Sons: Chichester and New York, 1981; Vol. 2.

(7) Mana, M. R.; Yarkony, D. R. *J. Chem. Phys.* **1993**, *99*, 5251. Yarkony, D. R. *J. Chem. Phys.* **1993**, *97*, 4407.

(8) Farazdel, A.; Dupuis, M. *J. Comput. Chem.* **1991**, *12*, 276.

(9) Bofill, J. M.; Anglada, J. M. *Theor. Chem. Acc.* **2001**, *105*, 463−472. Czerminski, R.; Elber, R. *J. Chem. Phys.* **1990**, *92*, 5580−5601.

(10) Shanno, D. F. *Math. Comput.* **1970**, *24*, 647. Goldfarb, D. *Math. Comput.* **1970**, *24*, 23. Fletcher, R. *Comput. J.* **1970**, *13*, 317. Broyden, C. G. *J. Inst. Math. Appl.* **1970**, *6*, 222.

(11) Anglada, J. M.; Bofill, J. M. *J. Comput. Chem.* **1997**, *18*, 992.

(12) AMPAC program, local version, extended by D. Liotard, 1987.

(13) Dewar, M. J. S.; Zoebisch, E. G.; Healy, E. F.; Stewart, J. J. P. *J. Am. Chem. Soc.* **1985**, *107*, 3902.

(14) Baker, J.; Bergon, D. *J. Comput. Chem.* **1993**, *14*, 1339. Baker, J. *J. Comput. Chem.* **1992**, *13*, 240. Baker, J. *J. Comput. Chem.* **1993**, *14*, 1085.

(15) Baker, J. *J. Comput. Chem.* **1997**, *18*, 1079.

(16) Banerjee, A.; Adams, N.; Simons, J.; Shepard, R. *J. Phys. Chem.* **1985**, *89*, 52.

(17) Lindh, R.; Bernhardsson, A.; Schütz, M. *Chem. Phys. Lett.* **1999**, *303*, 567−575.

(18) Lindh, R.; Bernhardsson, A.; Karlström, G.; Malmqvist, P.-Å. *Chem. Phys. Lett.* **1995**, *241*, 423−428.

(19) Andersson, K.; Barysz, M.; Bernhardsson, A.; Blomberg, M. R. A.; Carissan, Y.; Cooper, D. L.; Fülscher, M. P.; Gagliardi, L.; De Graaf, C.; Hess, B. A.; Hagberg, D.; Karlström, G.; Lindh, R.; Malmqvist, P.-Å.; Nakajima, T.; Neogrády, P.; Olsen, J.; Raab, J.; Roos, B. O.; Ryde, U.; Schimmelpfennig, B.; Schütz, M.; Seijo, L.; Serrano-Andrés, L.; Siegbahn, P. E. M.; Stålring, J.; Thorsteinsson, T.; Veryazov, V.; Widmark, P.-O. *MOLCAS*, Version 6.0; Lund University, Sweden, 2004.

(20) Veryazov, V.; Widmark, P.-O.; Serrano-Andrés, L.; Lindh, R.; Roos, B. O. *Int. J. Quantum Chem.* **2004**, *100*, 626−635. Karlström, G.; Lindh, R.; Malmqvist, P.-Å.; Roos, B. O.; Ryde, U.; Veryazov, V.; Widmark, P.-O.; Cossi, M.; Schimmelpfennig, B.; Neograd y, P.; Seijo, L. *Comput. Mater. Sci.* **2003**, *28*, 222−239.

(21) Fletcher, R. *Practical Methods of Optimization*; Wiley: New York, 1981.

(22) We chose the transformation matrix **T** to be unitary, even if it is not strictly necessary, so not to have to include the computation of the inverse matrix, which is anyway needed. By the way, we note that Anglada and Bofill implicitly affirm that **T** should be unitary when stating that $\mathbf{T}_b^T\mathbf{T}_b = \mathbf{I}_b$. By consequence, their statement that $[\mathbf{R}(\mathbf{r})]^T\mathbf{T}_b = \mathbf{I}_b$ is not correct, given the fact that $\mathbf{R}(\mathbf{r})$ is not, in general, unitary.

(23) Widmark, P.-O.; Malmqvist, P.-Å.; Roos, B. O. *Theor. Chem. Acc.* **1990**, *77*, 291−306. Roos, B. O.; Lindh, R.; Malmqvist, P.-Å.; Veryazov, V.; Widmark, P.-O. *J. Phys. Chem. A* **2004**, *108*, 2851−2858.

(24) Hariharan, P. C.; Pople, J. A. *Theor. Chim. Acta* **1973**, *28*, 213−222.

(25) Helbing, J.; Bregy, H.; Bredenbeck, J.; Pfister, R.; Hamm, P.; Huber, R.; Wachtveil, J.; De Vico, L.; Olivucci, M. *J. Am. Chem. Soc.* **2004**, *126*, 8823−8834.

(26) Müller, K.; Brown, L. D. *Theor. Chem. Acc.* **1979**, *53*, 75−93.

(27) Garavelli, M.; Page, C. S.; Celani, P.; Olivucci, M.; Schmid, W. E.; Trushin, S. A.; Fuss, W. *J. Phys. Chem. A* **2001**, *105*, 4458−4469.

(28) Migani, A.; Sinicropi, A.; Ferré, N.; Cembran, A.; Garavelli, M.; Olivucci, M. *Faraday Discuss.* **2004**, *127*, 179−191. Migani, A.; Robb, M. A.; Olivucci, M. *J. Am. Chem. Soc.* **2003**, *125*, 2804.

(29) Schuster, D. I. In *The chemistry of enones*; Petai, S., Rappoport, Z., Eds.; John Wiley and Sons: Chichester, U.K., 1989; Vol. 2, pp 693−756. Schuster, D. I. In *Rearrangements in ground and exited states*; de Mayo, P., Ed.; Academic Press: London, 1980; Vol. 3, pp 161−279.

(30) Reguero, M.; Olivucci, M.; Bernardi, F.; Robb, M. A. *J. Am. Chem. Soc.* **1994**, *116*, 2103-2114.

CT0500949